Available online at www.sciencedirect.com
SCIENCE DIRECT®
Journal of Sound and Vibration 284 (2005) 805–824
JOURNAL OF SOUND AND VIBRATION
www.elsevier.com/locate/jsvi

Vibration suppression of a cantilever beam using eddy current damper

Jae-Sung Bae[a,*], Moon K. Kwak[b], Daniel J. Inman[b]

[a]*Korea Institute of Energy Research, Wind Power/Fluid Machinery Research Center, 71-2, Jang-dong, Yuseong-gu, Daejeon 305-343, Korea*

[b]*Department of Mechanical Engineering, Center for Intelligent Material Systems and Structures, Virginia Tech 310 Durham Hall, Blacksburg, VA 24061, USA*

Received 8 March 2004; received in revised form 15 July 2004; accepted 18 July 2004
Available online 15 December 2004

Abstract

This paper is concerned with a new modeling technique for the effective eddy current damper and vibration suppression of a beam using the eddy current damper. The eddy current damper consists of the permanent magnets and the conducting sheet. The relative motion between the magnets and the conducting sheet produces eddy currents thus resulting in the electromagnetic force, which turns out to be the damping force thus suppressing vibrations. The important advantage of the proposed eddy current damper is that it does not require any electronic devices and external power supplies. In the present study, the theoretical model for the eddy current damper is derived using the electromagnetic theory combined with the image method. The theoretical model enables us to estimate the damping augmented to the host structure as well as develop a design tool for the eddy current damper. It is found from the comparison with the experimental results that the theoretical model can predict the damping characteristics and the dynamic behavior of the structure. The theoretical and experimental results also showed that the vibration of the beam can be successfully suppressed by means of the eddy current damper.

*Corresponding author. Tel.: +82 42 860 3376; fax: +82 42 860 3739.
E-mail addresses: jsbae@kier.re.kr (J.-S. Bae), kwakm@dongguk.edu (M.K. Kwak), dinman@vt.edu (D.J. Inman).

0022-460X/$ - see front matter © 2004 Published by Elsevier Ltd.
doi:10.1016/j.jsv.2004.07.031

Nomenclature

a	height of magnet
A	half-width of conducting sheet
b	width of magnet
$\mathbf{B}$	magnetic field
$\mathbf{E}$	electric field
$\mathbf{J}$	current density
l_e	distance between the beam end and the center of a magnet
m	mass of beam
u	displacement of beam
x	coordinates
t	time
δ	thickness of conducting sheet
ε_0	permittivity of free space
θ	rotation angle of eddy current damper
ρ	surface charge density
σ	conductivity
ω_{bi}	natural frequency of beam
ς_{bi}	damping ratio

1. Introduction

In modern vibration controller design for smart structures, much effort is devoted to the development of an efficient actuator along with high-performance control algorithms. Smart materials such as PZT, terfenol-D, ER, MR, and shape memory alloys have been exploited as candidates for actuators. In addition to these actuators, it is well known that the damping can be obtained by the electromagnetic force which is generated by the movement of a conducting material through a stationary magnet or the movement of a magnet through a stationary conducting material (Fig. 1). By Maxwell's law, a time-varying magnetic field produces an electric field. This causes "eddy" currents to flow in the conductor. These currents dissipate energy as they flow through the resistance of the conductor. The resulting drag force on the conductor is proportional to its velocity relative to the field. The device thus functions as a viscous damping element.

Eddy currents have been used in our home electric appliances, non-contact measurement devices, and brake systems for high-speed trains. The advantage of the eddy current brake systems [1–5] is that they are non-contacting devices, thus resulting in semi-permanent devices.

Karnopp [6] introduced that a linear electrodynamic motor consisting of copper wire with permanent magnets can be used as an electromechanical damper. He showed that his actuator could be much smaller and lighter than conventional actuators. Schmid and Varga [7] studied the vibration-reducing system with eddy current damping for high-resolution and nanotechnology devices such as an scanning tunneling microscope (STM). Larose et al. [8] studied the effectiveness of external means for reducing the oscillations of a full-bridge aeroelastic model. To reduce the oscillation, they used a tuned mass damper (TMD) that has the adjustable inherent damping provided by an eddy current mechanism. Okada et al. [9] studied the method of self-sensing active vibration control using a moving-coil-type actuator. They estimated the velocity from a driving current which is used to reduce the vibration. Teshima et al. [10] investigated the effects of an eddy current damper on the vibrational characteristics in the super-conducting levitation and showed that the damping in vertical vibration was about 100 times improved by eddy current dampers.

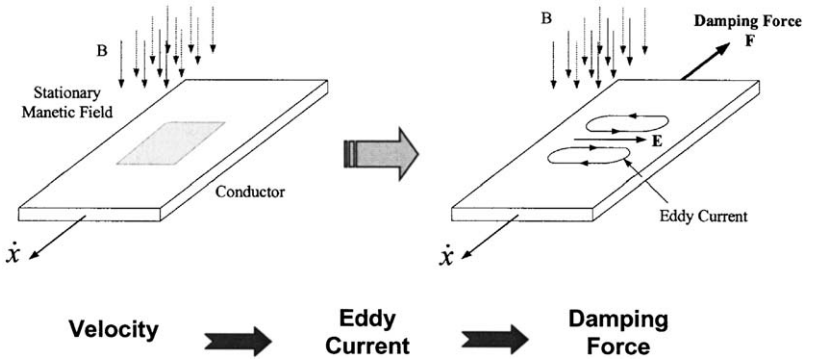

Fig. 1. Damping force due to eddy current.

Takagi et al. [11] studied thin plate deflection in a magnetic field analytically and experimentally. They used an electromagnet with very high current (several hundred Amperes) to generate the magnetic field. CSA Engineering Inc. [12] has studied a magnetic tuned mass damper for a spacecraft solar array and a magnetically damped isolation mount for space shuttle payload. Matsuzaki et al. [13] proposed the concept of a new vibration control system in which the vibration of the partially magnetized beam is suppressed by using the electromagnetic forces. They performed the vibration suppression analysis of the thin beam with the two magnetized segments subjected to an impulsive force to confirm the effectiveness of their system. Graves et al. [14] derived the mathematical models of electromagnetic dampers based on a motional electromagnetic field (emf) and transformer emf devices and presented a theoretical comparison between these two devices. A motional emf device provides a generated current due to the movement of a closed conduction circuit or a conductor through a stationary magnetic field. A transformer emf device generates an emf within a stationary conducting circuit, due to a time-varying magnetic field. Both these devices can also be used as a damper. Recently, Kwak et al. [15] investigated the effects of the eddy current damper on the cantilever beam and their experimental results showed that the eddy current damper can be an effective device for vibration suppression. However, they did not derive the detailed eddy current damping model and used a simple electromagnetic theory instead.

In the present study, a theoretical model for an eddy current damper is first derived based on the electromagnetic theory. To this end, the damping effect caused by the permanent magnet moving on an infinite conducting sheet is investigated. Since the conducting sheet used for the eddy current damper is finite in size, the end effect is taken into consideration by using the image method. Using the theoretical result on the eddy current damping model, the dynamic characteristics of the cantilever beam with the eddy current damper considered in Ref. [15] are investigated analytically and compared with the experimental result. It can be concluded that the damping value for the eddy current damping is theoretically predictable and the overall damping characteristics of the structure can be improved dramatically by the addition of the eddy current damper.

2. Modeling of eddy current damper

2.1. Infinitely extending conducting sheet

Fig. 2 shows a conducting sheet of thickness δ and conductivity σ that moves with constant velocity $\mathbf{v}$ in the air gap of a rectangular magnet. For simplicity, we assume that the width of the conducting sheet, A, is infinite or much larger than that of a pole, a, and then the effect of the boundary of the conductor can be negligible. The surface charges (Coulomb charge) are assumed to be generated at the end of the pole projection area on the conducting sheet as shown in Fig. 3. The current density induced by a moving conducting sheet at velocity $\mathbf{v}$ is given by [8,16,17]

$$\mathbf{J} = \sigma(\mathbf{E} + \mathbf{v} \times \mathbf{B}), \tag{1}$$

where $\mathbf{B} = B_z\mathbf{k}$ inside the pole projection area and $\mathbf{B} = 0$ outside. The $\mathbf{v} \times \mathbf{B}$ term is an electromotive field driving the eddy current $\mathbf{J}$. $\mathbf{E}$ is the electrostatic field of Coulomb charge induced within the conducting sheet along the edges of the footprint parallel to the motion of the sheet, as shown in Fig. 3.

Heald [2] and Schieber [17] have derived the eddy current distributions due to a rectangular electromagnet. They assumed that the rectangular electromagnet is moving with a constant velocity. The eddy current damper employed in Ref. [15] shows that the permanent magnet undergoes a pendulum motion. Due to the radial motion, the assumption of a constant velocity profile no longer holds. Hence, the linearly varying velocity along the x-axis in Fig. 3 is considered in the present study.

For the motion of the conducting sheet in the y-direction, the negative charges move leftward and are stacked at the left end of the pole projection. Similarly, the right ones move right and are stacked at the right end. Based on the magnetic pole density at the surface of the permanent magnet, the surface charge densities on the parallel to the yz plane at $x = \pm a$ can be written as

$$\rho_{sx+} = +\varepsilon_0 v_+ B_z, \tag{2}$$

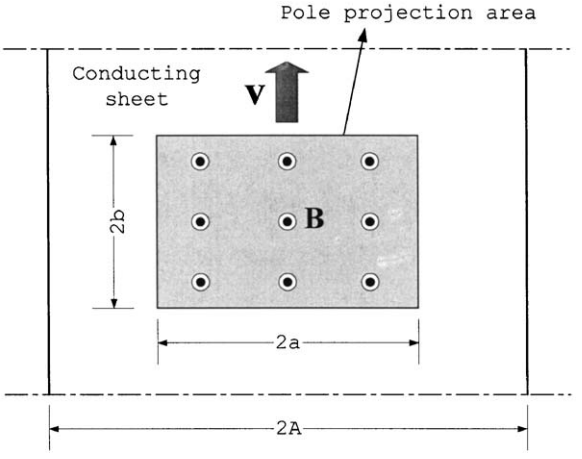

Fig. 2. Configuration of linearly moving conduction sheet.

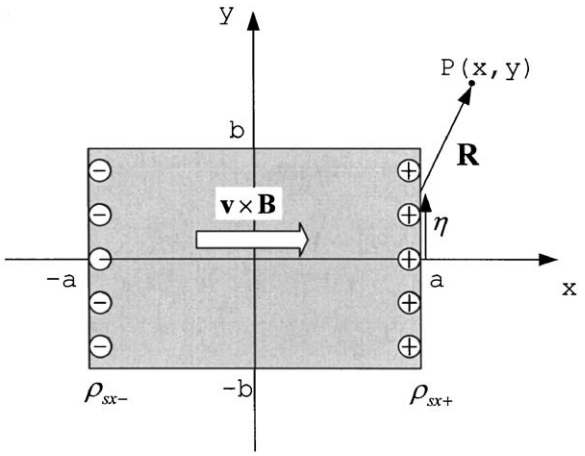

Fig. 3. Surface charge densities for the motion of conducting sheet.

$$\rho_{sx-} = -\varepsilon_0 v_- B_z, \tag{3}$$

where ε_0 is the permittivity of free space. $v_\pm$ are the velocities in the y-direction at $x = \pm a$. Using Coulomb's law, the incremental electric field $\mathrm{d}E_{x+}$ in the x-direction at $P(x, y)$ due to the incremental charge $\rho_{sx+}\,\mathrm{d}\eta$ is

$$\mathrm{d}E_{x+} = \frac{\rho_{sx+}}{2\pi\varepsilon_0 R}\,\frac{x-a}{R}\,\mathrm{d}\eta, \tag{4}$$

where a is the height of a rectangular magnet, η is a location in the y-direction at $x = \pm a$, and $R = |\mathbf{R}| = \sqrt{(x-a)^2 + (y-\eta)^2}$. Substituting Eqs. (2) and (3) into Eq. (4) and integrating from $-b$ to b, the electric field at $P(x, y)$ due to the positive charge is

$$E_x = -\frac{v_+ B_z}{2\pi}\left(\tan^{-1}\frac{y-b}{x-a} - \tan^{-1}\frac{y+b}{x-a}\right) + \frac{v_- B_z}{2\pi}\left(\tan^{-1}\frac{y-b}{x+a} - \tan^{-1}\frac{y+b}{x+a}\right), \tag{5}$$

where the electric field in the y-direction is assumed to be negligible.

Substituting Eq. (5) into Eq. (1), the current density on the conducting sheet is

$$J_x = \begin{cases} \sigma(E_x + vB_z) & \text{inside,} \\ \sigma E_x & \text{outside.} \end{cases} \tag{6}$$

Then the damping force can be calculated by

$$\mathbf{F} = \int_V \mathbf{J} \times \mathbf{B}\,\mathrm{d}V. \tag{7}$$

Substituting Eqs. (5) and (6) into Eq. (7), the damping force is

$$F_y = -\sigma\delta B_z^2 S v_0 \alpha_1, \tag{8}$$

$$\alpha_1 = 1 - \frac{1}{2\pi}\left[4\tan^{-1}\frac{b}{a} + \frac{b}{a}\ln\left(1+\frac{a^2}{b^2}\right) - \frac{a}{b}\ln\left(1+\frac{b^2}{a^2}\right)\right], \tag{9}$$

where S $(= 4ab)$ is the pole projection area and $v_0 (= (v_+ + v_-)/2)$ is the mean velocity. The second term of α_1 represents the effect of the surface charge on the eddy current damping force. Eqs. (8) and (9) can be used to calculate the damping force of a conducting sheet with an infinite width. Eqs. (8) and (9) are derived on the assumption that the conducting sheet is moving with linearly varying velocity. However, it is found that it provides the same result as given in Refs. [2,7], since the resulting equation is expressed in terms of the mean velocity.

2.2. Image method and imaginary eddy current

For a conductor with a finite width, the boundary conditions need to be considered since the x component of the eddy current is zero at the left and right edges of the conducting sheet. An imaginary eddy current and an image method [18] are introduced to satisfy the boundary condition in this study.

By introducing imaginary eddy currents, the net eddy current J' can be written as

$$J' = J_x^{(1)} - J_x^{(2)} - J_x^{(3)}, \tag{10}$$

where the primary eddy current $J_x^{(1)}$ is the eddy current of the infinite conducting sheet in Eq. (6). $J_x^{(2)}$ and $J_x^{(3)}$ are the imaginary eddy currents at the right and left sides of the conductor, respectively, as shown in Fig. 4. To be more complete, the infinite number of the imaginary eddy currents should be considered but, for simplicity, the pair of the imaginary eddy currents, like $J_x^{(2)}$ and $J_x^{(3)}$, are considered in the present study.

The net eddy current must be zero at the edges of the conductor ($x = \pm A$). The idea to find the imaginary eddy current is to assume that it is symmetric to the primary eddy current $J_x^{(1)}$ at the right and left sides of the conductor. As shown in Fig. 4, the right imaginary eddy current $J_x^{(2)}$ is symmetric to the primary eddy current $J_x^{(1)}$ at the axis of $x = A$. Hence, we know that the relation is

$$J_x^{(2)}(x, y) = J_x^{(1)}(2A - x, y). \tag{11}$$

Similarly, the left imaginary eddy current $J_x^{(3)}$ can be written as

$$J_x^{(3)}(x, y) = J_x^{(1)}(-2A - x, y). \tag{12}$$

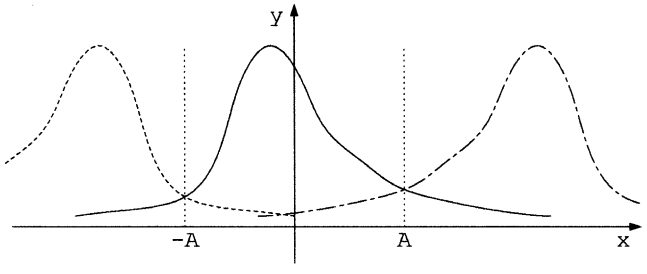

Fig. 4. Symmetry of imaginary eddy currents: ——, $J_x^{(1)}$; – – –, $J_x^{(2)}$; ....., $J_x^{(3)}$.

Therefore, we can calculate the net eddy current distributions on the finite conducting sheet to substitute Eqs. (11) and (12) into Eq. (10).

2.3. Finite conducting sheet with linearly varying velocity

From Eqs. (11) and (12), the right and left imaginary eddy current distributions inside the pole projection area are

$$J_x^{(2)} = \sigma B_z \left\{ \frac{1}{2\pi} \left[v_+ \left(\tan^{-1} \frac{y-b}{x+a-2A} - \tan^{-1} \frac{y+b}{x+a-2A} \right) + v_- \left(-\tan^{-1} \frac{y-b}{x-a-2A} + \tan^{-1} \frac{y+b}{x-a-2A} \right) \right] \right\}, \tag{13}$$

$$J_x^{(3)} = \sigma B_z \left\{ \frac{1}{2\pi} \left[v_+ \left(\tan^{-1} \frac{y-b}{x+a+2A} - \tan^{-1} \frac{y+b}{x+a+2A} \right) + v_- \left(-\tan^{-1} \frac{y-b}{x-a+2A} + \tan^{-1} \frac{y+b}{x-a+2A} \right) \right] \right\}. \tag{14}$$

The damping force can be derived as

$$F_y = -\int_{-b}^{b} \int_{-a}^{a} (J_x^{(1)} - J_x^{(2)} - J_x^{(3)}) B_0 \, \mathrm{d}x \, \mathrm{d}y = F_y^{(1)} + F_y^{(2)} + F_y^{(3)}. \tag{15}$$

The integrations of the three terms in Eq. (15) are expressed as

$$F_y^{(1)} = -\sigma \delta v_0 B_z^2 S \left\{ 1 - \frac{1}{2\pi} \left[4\tan^{-1} h + h \log\left(1 + \frac{1}{h^2} \right) - \frac{1}{h} \log(1+h^2) \right] \right\}, \tag{16}$$

$$F_y^{(2)} = \frac{\sigma \delta B_z^2 S}{2\pi} \left[\frac{1}{2} v_+ I_1 + \frac{1}{2} v_- I_2 \right], \tag{17}$$

$$F_y^{(3)} = \frac{\sigma \delta B_z^2 S}{2\pi} \left[\frac{1}{2} v_+ I_2 + \frac{1}{2} v_- I_1 \right], \tag{18}$$

where $h = b/a$. The details of the integrations I_1 and I_2 are explained in Appendix A. Therefore, the damping force due to the net eddy current is

$$F_y = -\sigma \delta v_0 B_z^2 S(\alpha_1 + \alpha_2), \tag{19}$$

where α_2 represents the end effect of the conducting sheet on the damping force and is defined as

$$\alpha_2 = -\frac{1}{2\pi}(I_1 + I_2). \tag{20}$$

In the previous work [15], both the effect of the surface charge and the end effect were not considered.

3. Modeling of cantilever beam with ECD

Fig. 5 shows a cantilever beam with an ECD at its end [15]. Their theoretical developments are summarized below.

The equations of motion can be obtained as

$$M\ddot{\eta} + C\dot{\eta} + K\eta = B_f F, \tag{21}$$

where

$$M = \begin{bmatrix} M_t & \bar{\Phi}^{\mathrm{T}} \\ \bar{\Phi} & J_e \end{bmatrix}, \quad C = \begin{bmatrix} C_b & 0 \\ 0 & C_e \end{bmatrix}, \quad K = \begin{bmatrix} K_b & 0 \\ 0 & k_e \end{bmatrix}, \quad B_f = \begin{Bmatrix} \Phi_L^{\mathrm{T}} \\ 0 \end{Bmatrix}, \quad \eta = \begin{Bmatrix} q \\ \theta \end{Bmatrix}. \tag{22}$$

C_b is the damping matrix of the beam and

$$M_t = m\int_0^L \Phi^{\mathrm{T}}\Phi \,\mathrm{d}x + M_C\Phi_L^{\mathrm{T}}\Phi_L + M_e[\Phi_L + l_e\Phi'_L]^{\mathrm{T}}[\Phi_L + l_e\Phi'_L], \tag{23}$$

$$\bar{\Phi} = M_e l_e[\Phi_L + l_e\Phi'_L], \; J_e = M_e l_e^2, \tag{24}$$

$$K_b = EI\int_0^L \Phi''^{\mathrm{T}}\Phi'' \,\mathrm{d}x, \quad \Phi_L = \Phi(L), \tag{25}$$

$$\Phi'_L = \frac{\mathrm{d}^2\Phi(L)}{\mathrm{d}x^2}. \tag{26}$$

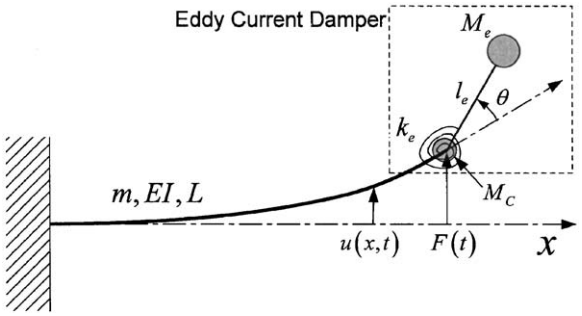

Fig. 5. Cantilever beam with eddy current damper at the beam end.

For the proposed eddy current damper, the mean velocity in Eq. (19) is

$$v_0 = l_e\dot{\theta}. \tag{27}$$

The damping coefficient in Eq. (22) is then

$$C_e = \sigma\delta l_e B_z^2 S(\alpha_1 + \alpha_2). \tag{28}$$

Ignoring the damping term and the ECD term in Eq. (21) and solving the eigenvalue problem, we can obtain the transformation

$$\eta = Uq. \tag{29}$$

The matrix U satisfies the orthogonal relationships such as

$$U^{\mathrm{T}} M_t U = I, \quad U^{\mathrm{T}} K_b U = \Lambda_b, \tag{30}$$

where I is the $n \times n$ unit matrix and

$$\Lambda_b = \mathrm{diag}(\omega_{b1}^2 \;\; \omega_{b2}^2 \;\; \cdots \;\; \omega_{bn}^2). \tag{31}$$

The damping matrix C_b is assumed to be

$$U^{\mathrm{T}} C_b U = 2Z_b\Omega_b, \tag{32}$$

where

$$Z_b = \mathrm{diag}(\zeta_{b1} \;\; \zeta_{b2} \;\; \cdots \;\; \zeta_{bn}), \tag{33}$$

$$\Omega_b = \sqrt{\Lambda_b}. \tag{34}$$

Let us introduce the state vector

$$z = [q \;\; \theta/L \;\; \dot{q} \;\; \dot{\theta}/L]^{\mathrm{T}}. \tag{35}$$

Substituting Eqs. (29), (33), (34), and 44 into Eq. (21), we obtain

$$M^*\ddot{z} + C^*\dot{z} + K^* z = B_f^* F, \tag{36}$$

where

$$M^* = \begin{bmatrix} I & \bar{\Phi}^{*\mathrm{T}} \\ \bar{\Phi}^* & 1 \end{bmatrix}, \tag{37a}$$

$$C^* = \begin{bmatrix} 2Z_b\Omega_b & 0 \\ 0 & 2\zeta_e\omega_e \end{bmatrix}, \tag{37b}$$

$$K^* = \begin{bmatrix} \Lambda_b & 0 \\ 0 & \omega_e \end{bmatrix}, \tag{37c}$$

$$B_f^* = \begin{Bmatrix} U^{\mathrm{T}}\Phi_L^{\mathrm{T}} \\ 0 \end{Bmatrix}. \tag{37d}$$

The final state-space equation is then

$$\dot{y} = A_s y + B_s F, \tag{38}$$

where

$$y = [z^{\mathrm{T}} \quad \dot{z}^{\mathrm{T}}]^{\mathrm{T}}, \tag{39}$$

$$A_s = \begin{bmatrix} 0 & I \\ -M^{*-1}K & -M^{*-1}C \end{bmatrix}, \tag{40a}$$

$$B_s = \begin{Bmatrix} 0 \\ M^{*-1}B_f^* \end{Bmatrix}. \tag{40b}$$

4. Numerical analysis

4.1. Rectangular pole with constant velocity

For the pole with a constant velocity, the positive and negative velocities in Eq. (5) are the same as v_0. Fig. 6 shows the current density distribution on the conducting sheet in Eq. (6) for the case of $y = 0$, $h = 0.5$, and $w(A/a) = 1.5$. The pole projection area is from $x/a = -1.0$ to 1.0. The dash–dotted line is the current distribution generated by the motion of the conductor and the dotted line is the current distribution due to the surface charge. The solid line is the primary current density distribution. It can be readily seen that the current density is considerably decreased by the surface charge.

Fig. 7 shows the primary and imaginary electric field distributions on the moving conduction sheet. The dotted line and dash–dotted line are the density distributions due to the right and left

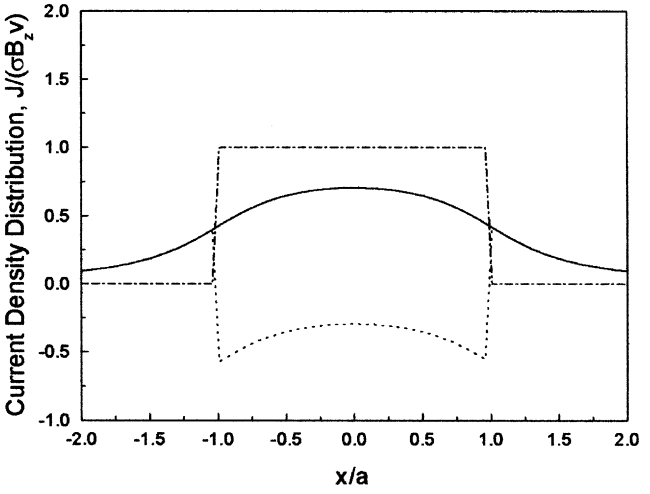

Fig. 6. Current density distribution of a conducting sheet with constant velocity ($y = 0$, $h = 0.5$, $w = 1.5$): ——, $J_x^{(1)}$; ....., E_x; – - –, $v \times B$.

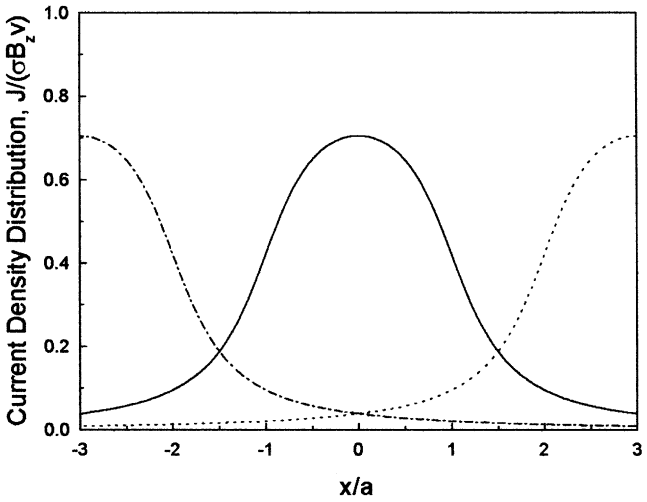

Fig. 7. Primary and imaginary eddy current distributions ($y = 0,\ h = 0.5,\ w = 1.5$): ——, $J_x^{(1)}$; ....., $J_x^{(2)}$; – – –, $J_x^{(3)}$.

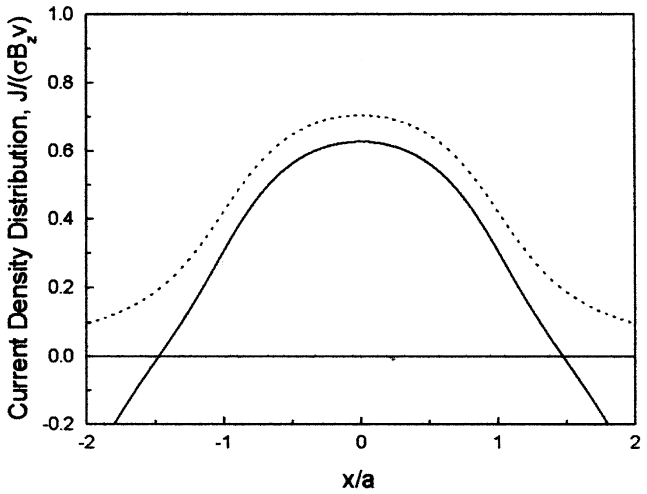

Fig. 8. Net eddy current distributions of finite and infinite conducting sheets: ——, finite sheet; ....., infinite sheet.

imaginary electric fields, respectively. The net current density on the pole projection area is obtained by the summation of these primary and imaginary current distributions. At the end of the conducting sheeting, $x/a = -1.5$ and 1.5, the current density of the imaginary current density is the same as that of the primary one. Fig. 8 shows the end effect of the conducting sheet on the current distributions. Due to the existence of the edge, the net current density is considerably decreased. At $x/a = -1.5$ and 1.5, the current density should be zero, but the present results is not exactly zero. This is because the one pair of the imaginary current distribution is considered in the present study for simplicity. Fig. 9 shows the three-dimensional net current density distribution J'

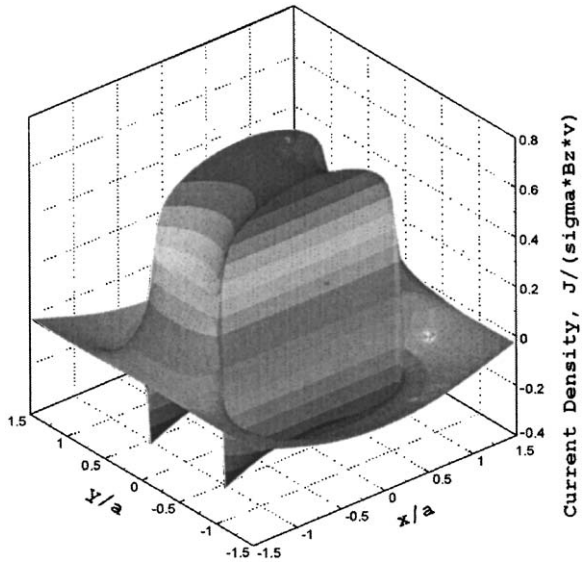

Fig. 9. Three-dimensional net current distribution ($h = 0.5,\ w = 1.5$).

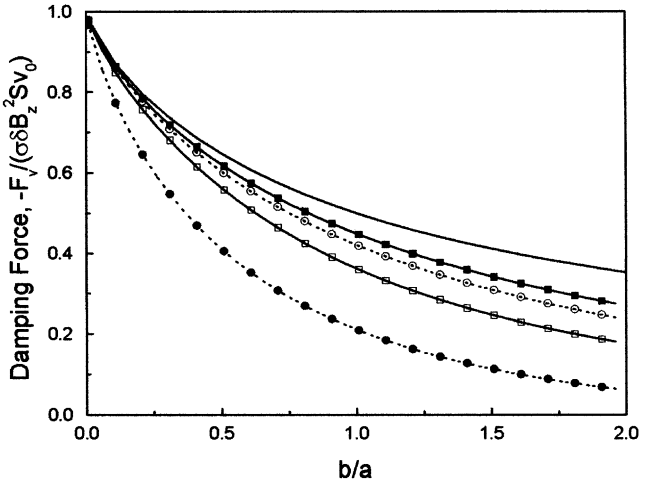

Fig. 10. Effects of edge on eddy current damping force: ——, infinite end; —■—, $A/a = 2.5$; .....○....., $A/a = 2.0$; —□— , $A/a = 1.5$; ·····●·····, $A/a = 1.0$.

on the conducting sheet with a constant velocity. In the y-direction, the current density at the edge is larger than that at the center. Hence, it can be readily seen that the current density increases as the aspect ratio h decreases.

Fig. 10 shows the damping forces acting on the moving conducting sheet due to the rectangular pole. As the aspect ratio b/a of the pole decreases, the damping force increases. As the w increases, the damping force increases. When the aspect ratio is 0.2 and the width ratio is 1.0, the ratios of the damping forces with and without end effect are 0.65 and 0.80, respectively.

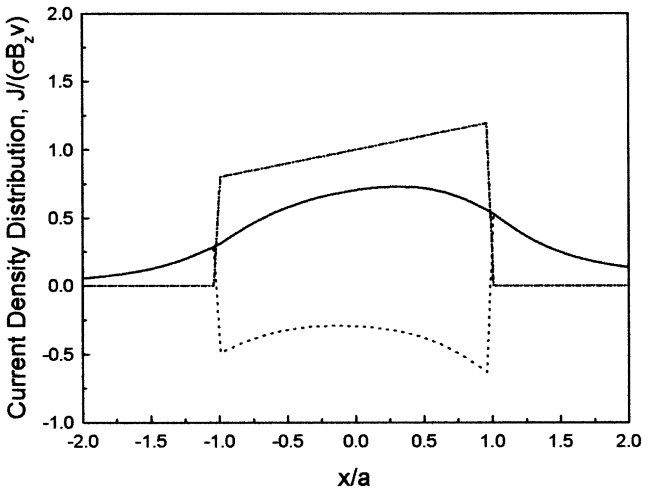

Fig. 11. Current density distribution of a conductor with linearly varying velocity ($y = 0,\ h = 0.5,\ w = 1.5,\ a/R = 0.2$): ——, J_x^1; ....., E_x; – – –, $v \times B$.

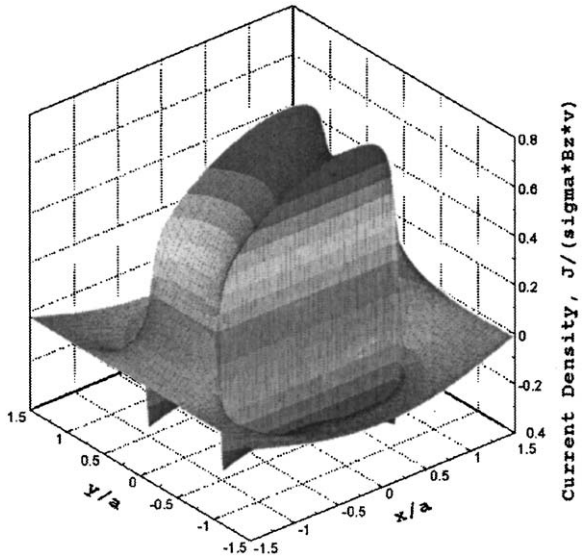

Fig. 12. Three-dimensional net current density distribution ($h = 1.5,\ w = 1.5,\ a/R = 0.2$).

4.2. Rectangular pole with linearly varying velocity

Fig. 11 shows the current density distribution on the conducting sheet moving with a linearly varying velocity along the x-axis for the case of $y = 0,\ h = 0.5$, and $a/l_e = 0.2$. Fig. 12 shows the three-dimensional net current distribution of the conducting sheet. Due to a linearly varying velocity, the current distribution is no longer symmetric about the center of the pole. From

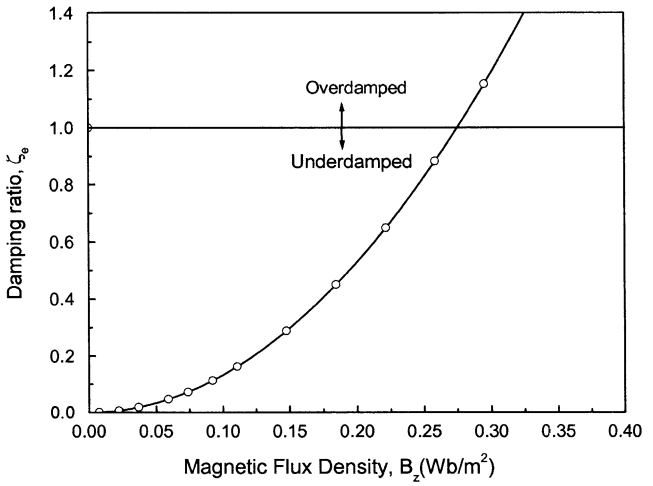

Fig. 13. Damping ratio of eddy current damper.

Eq. (19), we know that the damping force is independent of the radius ratio a/l_e. Hence, the current distribution is not symmetric but the net damping force due to the pole is the same as the previous case, as shown in Fig. 9.

Fig. 13 shows the damping ratio of the eddy current damper. The damping ratio due to the ECD is defined as

$$\zeta_e = \frac{C_e}{2\sqrt{k_e J_e}}. \tag{42}$$

When the magnetic flux density is greater than 0.275 Wb/m^2, the eddy current damper has "overdamped motion" [19]. Overdamped motion means that the damping ratio is greater than 1.0 and the overdamped system does not oscillate. From Fig. 13, we know that it is possible to obtain very large viscous damping from the eddy current damper. Thus, the eddy current damper can be used as an effective vibration absorber.

4.3. Dynamic characteristics of cantilever beam

The ECD was built to show its effectiveness on the vibration suppression of the beam in Ref. [15]. Fig. 14 shows the aluminum beam with the ECD [15]. The ECD consists of a copper plate and rectangular permanent magnets as shown in Fig. 14. The aluminum plate to which the magnets are attached is bolted to the beam end by the stainless plate. The mass of the ECD is 0.15 kg. The fundamental frequencies of the beam without ECD and non-activated ECD are 10 and 3.2 Hz, respectively. Numerical simulations on the beam with the eddy current damper shown in Fig. 5 have been performed. The length L, mass m, and the bending stiffness EI of the beam are 0.39 m, 0.087 kg, and 1.84 N m^2, respectively. Fig. 15 shows the frequency responses of the original beam and the beam with non-activated ECD. The fundamental natural frequency of the original beam is 10.5 Hz and the beam with ECD is 3.3 Hz. Due to the increase of

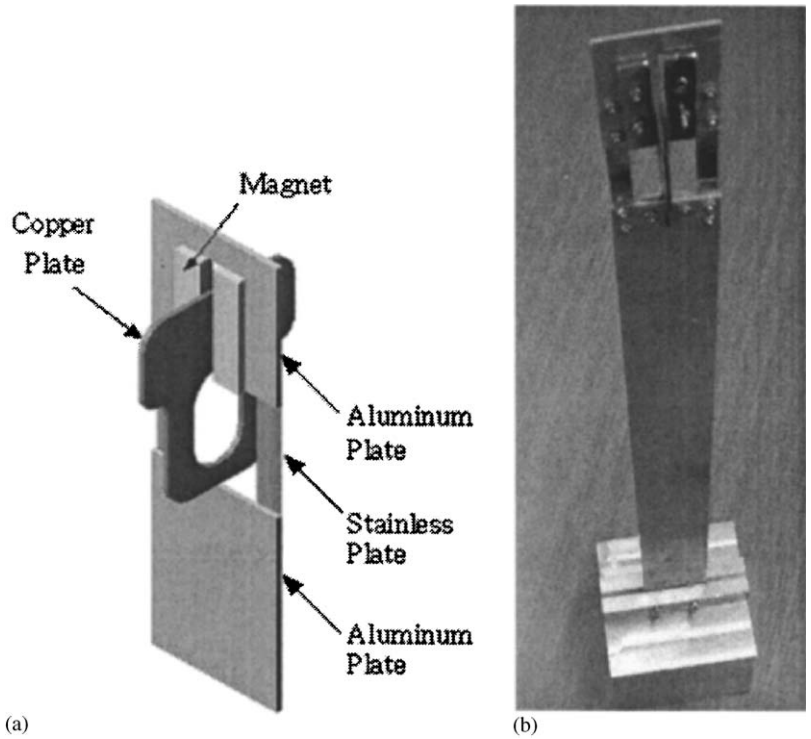

Fig. 14. Aluminum beam with eddy current damper: (a) eddy current damper, (b) cantilever beam with ECD.

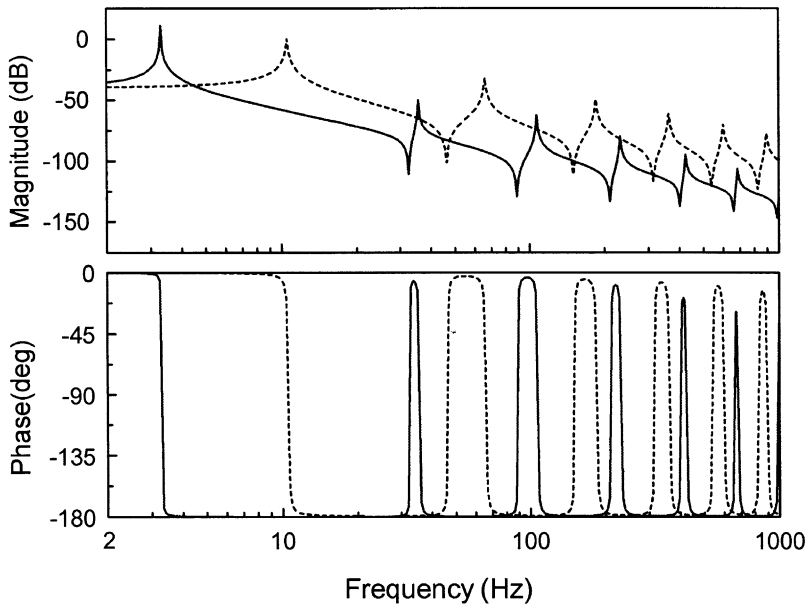

Fig. 15. Frequency response plots of beam with and without ECD: ——, with ECD; ....., without ECD.

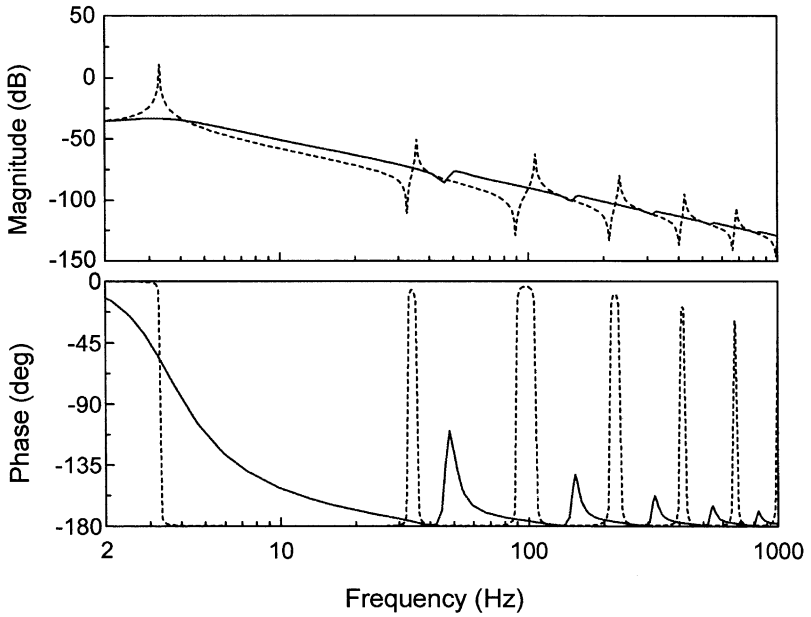

Fig. 16. Frequency response plots: ——, ECD on; ....., ECD off.

the tip mass, the fundamental frequency is considerably decreased and the response magnitude is increased.

Fig. 16 shows the frequency responses of the beam when the ECD is activated. When the ECD is activated, the damping of the beam increases dramatically through the entire frequency range. Fig. 17 shows the numerical and experimental time responses of the beam with ECD. The present numerical simulation agrees well with the experimental time response [15]. Due to the activation of ECD, the vibration is quickly suppressed. When the beam oscillates, the relative motion of the magnet generates the eddy current on the conducting sheet and its electromagnetic force dissipates the vibration energy of the beam. Hence, the ECD proposed in the present study is very effective in the vibration suppression of the beam.

5. Discussion and conclusions

In the present study, the theoretical model for the eddy current damper (ECD) was derived by using electromagnetic theory. The theoretical model can be used for the prediction of a damping value induced by the eddy current so that the design of an effective ECD for vibration suppression can be achieved in the preliminary design stage. The theoretical ECD model is based on the permanent magnet moving on a finite conducting sheet. To this end, the theoretical ECD model for the permanent magnet moving on an infinite conducting sheet was first considered and the result was later extended to the case of the finite conducting sheet. Since the ECD considered in Ref. [15] undergoes a pendulum motion, the linearly time-varying velocity was considered.

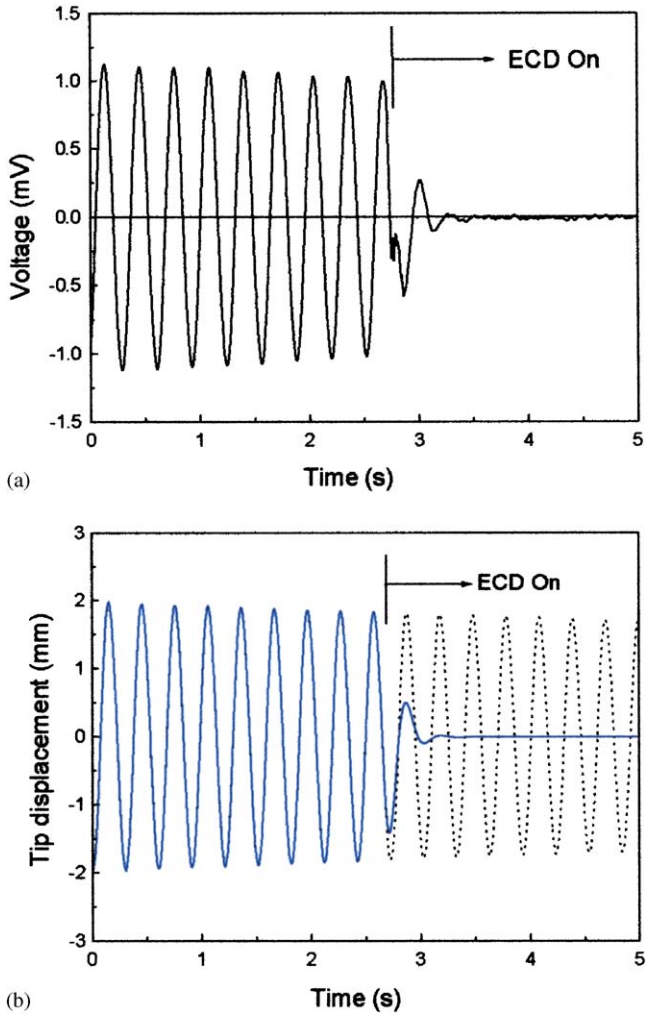

Fig. 17. Numerical and experimental time responses of beam with ECD: (a) time history of tip acceleration (experiment [15]); (b) time history of tip displacement (theory): ——, ECD on; ....., ECD off.

However, the net damping value for this case is identical to the case of constant velocity, which is in fact the mean velocity.

The proposed ECD model was used to predict the dynamic characteristics of the cantilever beam with the ECD considered in Ref. [15]. It must be noted here again that the damping value was not theoretically estimated in Ref. [15]. We used the material constants given by the permanent magnet production company to estimate the damping value of the ECD. It turns out that the theoretical result is reasonably close to the experimental result, thus validating the theoretical model. The theoretical time response of the cantilever beam with the ECD was compared to the experimental result of Ref. [15]. It shows that we can estimate the dynamic response accurately. As concluded in Ref. [15], the damping characteristics of the structure can be dramatically improved by the addition of the ECD so that vibration suppression can be easily achieved.

Acknowledgements

This work was supported by the Post-doctoral Fellowship Program of the Korea Science & Engineering Foundation (KOSEF) and partially by Dongguk University Research Fund. These supports are gratefully acknowledged.

Appendix A. Integrations

To calculate the damping generated by the right imaginary eddy current $J_x^{(2)}$, we utilize the relations

$$\int_{-b}^{b}\int_{-a}^{a}\tan^{-1}\frac{y-b}{x+a-2A}\,\mathrm{d}x\,\mathrm{d}y=\int_{-b}^{b}\int_{-a}^{a}-\tan^{-1}\frac{y+b}{x+a-2A}\,\mathrm{d}x\,\mathrm{d}y, \tag{A.1}$$

$$\int_{-b}^{b}\int_{-a}^{a}-\tan^{-1}\frac{y-b}{x-a-2A}\,\mathrm{d}x\,\mathrm{d}y=\int_{-b}^{b}\int_{-a}^{a}\tan^{-1}\frac{y+b}{x-a-2A}\,\mathrm{d}x\,\mathrm{d}y. \tag{A.2}$$

The integrations of Eqs. (A.1) and (A.2) are

$$\begin{aligned}I_1&=\frac{1}{ab}\int_{-b}^{b}\int_{-a}^{a}\tan^{-1}\frac{y-b}{x+a-2A}\,\mathrm{d}x\,\mathrm{d}y\\&=\frac{1}{ab}\left\{4Ab\tan^{-1}\frac{b}{A}-4(a-A)b\tan^{-1}\frac{b}{a-A}+A^2\log(4A^2)\right.\\&\quad-(A^2-b^2)\log[4(A^2+b^2)]-(a-A)^2\log[4(a-A)^2]\\&\quad\left.+[(a-A)^2-b^2]\log[4(a-A)^2+4b^2]\right\}\end{aligned} \tag{A.3}$$

and

$$\begin{aligned}I_2&=\frac{1}{ab}\int_{-b}^{b}\int_{-a}^{a}-\tan^{-1}\frac{y-b}{x-a-2A}\,\mathrm{d}x\,\mathrm{d}y\\&=\frac{1}{ab}\left\{4Ab\tan^{-1}\frac{b}{A}-4(a+A)b\tan^{-1}\frac{b}{a+A}+A^2\log(4A^2)\right.\\&\quad-(A^2-b^2)\log[4(A^2+b^2)]-(a+A)^2\log[4(a+A)^2]\\&\quad\left.+[(a+A)^2-b^2]\log[4(a+A)^2+4b^2]\right\}.\end{aligned} \tag{A.4}$$

The damping force generated by the right imaginary eddy current is then

$$\begin{aligned}F_y^{(2)}&=\frac{\sigma\delta\dot{\theta}l_eB_z^2S}{2\pi}\left[\frac{1}{2}\left(1+\frac{a}{l_e}\right)I_1+\frac{1}{2}\left(1-\frac{a}{l_e}\right)I_2\right]\\&=\frac{\sigma\delta\dot{\theta}l_eB_z^2S}{2\pi}\left[\frac{1}{2}(I_1+I_2)+\frac{a}{2l_e}(I_1-I_2)\right],\end{aligned} \tag{A.5}$$

where

$$I_1 = 4w\tan^{-1}\frac{h}{w} - 4(1-w)\tan^{-1}\frac{h}{1-w} + \frac{w^2}{h}\log w^2 - \frac{1}{h}(w^2-h^2)\log(w^2+h^2) - \frac{1}{h}(1-w)^2\log(1-w)^2 + \frac{1}{h}[(1-w)^2-h^2]\log[(1-w)^2+h^2], \tag{A.6}$$

$$I_2 = 4w\tan^{-1}\frac{h}{w} - 4(1+w)\tan^{-1}\frac{h}{1+w} + \frac{w^2}{h}\log w^2 - \frac{1}{h}(w^2-h^2)\log(w^2+h^2) - \frac{1}{h}(1+w)^2\log(1+w)^2 + \frac{1}{h}[(1+w)^2-h^2]\log[(1+w)^2+h^2]. \tag{A.7}$$

In Eqs. (A.6) and (A.7), $w = A/a$. From Eqs. (A.1)–(A.4), we know that

$$\int_{-b}^{b}\int_{-a}^{a}\tan^{-1}\frac{y-b}{x+a+2A}\,dx\,dy = \int_{-b}^{b}\int_{-a}^{a}-\tan^{-1}\frac{y-b}{x-a-2A}\,dx\,dy = I_2ab, \tag{A.8}$$

$$\int_{-b}^{b}\int_{-a}^{a}-\tan^{-1}\frac{y-b}{x-a+2A}\,dx\,dy = \int_{-b}^{b}\int_{-a}^{a}\tan^{-1}\frac{y-b}{x+a-2A}\,dx\,dy = I_1ab. \tag{A.9}$$

The damping force generated by the left imaginary eddy current is then

$$F_y^{(3)} = \frac{\sigma\delta\dot{\theta}l_eB_z^2S}{2\pi}\left[\frac{1}{2}\left(1+\frac{a}{l_e}\right)I_2 + \frac{1}{2}\left(1-\frac{a}{l_e}\right)I_1\right] = \frac{\sigma\delta\dot{\theta}l_eB_z^2S}{2\pi}\left[\frac{1}{2}(I_1+I_2) + \frac{a}{2l_e}(I_2-I_1)\right]. \tag{A.10}$$

References

[1] H.H. Wiederick, N. Gauthier, D.A. Campbell, Magnetic braking: simple theory and experiment, *American Journal of Physics* 55 (1987) 500–503.

[2] M.A. Heald, Magnetic braking: improved theory, *American Journal of Physics* 56 (1988) 521–522.

[3] L.H. Cadwell, Magnetic damping: analysis of an eddy current brake using an airtrack, *American Journal of Physics* 64 (1996) 917–923.

[4] K.J. Lee, K.J. Park, A contactless eddy current brake system. *IEEE Conference on Intelligent Processing Systems*, Australia, December 1998, pp. 193–197.

[5] K.J. Lee, K.J. Park, Optimal robust control of a contactless brake system using an eddy current, *Mechatronics* 9 (1999) 615–631.

[6] D. Karnopp, Permanent magnet linear motors used as variable mechanical damper for vehicle suspensions, *Vehicle System Dynamics* 18 (1989) 187–200.

[7] M. Schmid, P. Varga, Analysis of vibration-isolating systems for scanning tunneling microscopes, *Ultramicroscopy* 42–44 (1992) 1610–1615.

[8] G.L. Larose, A. Larsen, E. Svensson, Modeling of tuned mass dampers for wind-tunnel tests on a full-bridge aeroelastic model, *Journal of Wind Engineering and Industrial Aerodynamics* 54/55 (1995) 427–437.
[9] Y. Okada, K. Matuda, H. Hashitani, Self-sensing active vibration control using the moving-coil-type actuator, *Journal of Vibration and Acoustics* 117 (1995) 411–415.
[10] H. Teshima, M. Tanaka, K. Miyamoto, K. Nohguchi, K. Hinata, Effect of eddy current dampers on the vibrational properties in superconducting levitation using melt-processed YbaCuO bulk superconductors, *Physic C* 274 (1997) 17–23.
[11] T. Takagi, J. Tani, S. Matsuda, S. Kawamura, Analysis and experiment of dynamic deflection of a thin plate with a coupling effect, *IEEE Transactions on Magnetics* 28 (1992) 1259–1262.
[12] CSA Engineering Inc., http://www.csaengineering.com.
[13] Y. Matsuzaki, Y. Ishikubo, T. Kamita, T. Ikeda, Vibration control system using electromagnetic forces, *Journal of Intelligent Material Systems and Structures* 8 (1997) 751–756.
[14] K.E. Graves, D. Toncich, P.G. Iovenitti, Theoretical comparison of motional and transformer EMF device damping efficiency, *Journal of Sound Vibration* 233 (2000) 441–453.
[15] M.K. Kwak, M.I. Lee, S. Heo, Vibration suppression using eddy current damper, *Korean Society for Noise and Vibration Engineering* 13 (10) (2003) 760–766.
[16] D.K. Cheng, *Field and Wave Electromagnetics*, Addison-Wesley Publishing Company, Reading, MA, 1992.
[17] D. Schiber, Optimal dimensions of rectangular electromagnet for braking purpose, *IEEE Transactions on Magnetics* MAG-11 (1975) 948–952.
[18] K. Lee, K. Park, Eddy currents modeling with the consideration of the magnetic Reynolds number, in: *Proceedings of 2001 IEEE International Symposium on Industrial Electronics*, Pusan, Korea, June 2001, pp. 678–683.
[19] D.J. Inman, *Engineering Vibration*, Prentice-Hall, Englewood Cliffs, NJ, 1994.